Dependence of Shell Mix on Feedthrough in Direct Drive Inertial Confinement Fusion

S. P. Regan, J. A. Delettrez, V. N. Goncharov, F. J. Marshall, J. M. Soures, V. A. Smalyuk, P. B. Radha, B. Yaakobi, R. Epstein, V. Yu. Glebov, P. A. Jaanimagi, D. D. Meyerhofer,* T. C. Sangster, W. Seka, S. Skupsky, and C. Stoeckl
Laboratory for Laser Energetics, University of Rochester, 250 East River Road, Rochester, New York 14623-1299, USA

D. A. Haynes, Jr.
Los Alamos National Laboratory, Los Alamos, New Mexico 87545, USA

J. A. Frenje, C. K. Li, R. D. Petrasso, and F. H. Séguin
Plasma Science and Fusion Center, Massachusetts Institute of Technology, Cambridge, Massachusetts 02139, USA
(Received 21 May 2003; published 5 May 2004)

The mixing of cold, high-density shell plasma with the low-density, hot spot plasma by the Rayleigh-Taylor instability in inertial confinement fusion is experimentally shown to correlate with the calculated perturbation feedthrough from the ablation surface to the inner shell surface. A fourfold decrease in the density of shell material in the mix region of direct drive implosions of gas filled spherical plastic shells having predicted convergence ratios ~15 was observed when laser imprint levels were reduced and the initial shell was thicker, corresponding to a reduction in the feedthrough rms level by a factor of 6. Shell mix is also shown to limit the spherical compression of the implosion.

DOI: 10.1103/PhysRevLett.92.185002 PACS numbers: 52.70.La, 52.35.Py, 52.50.Jm

Inertial confinement fusion (ICF) occurs when a spherical shell target containing thermonuclear fuel is imploded [1,2]. During an implosion of a D_2 or DT gas filled plastic (CH) shell target, the shell is accelerated inward to a velocity of $\sim 10^7$ cm/s, and pressures ~10 Gbar are generated [3] as the shell is brought to peak compression with a deceleration reaching $\sim 10^{17}$ cm/s^2. ICF target acceleration and deceleration are realized when hot, low-density plasma pushes against cold, high-density plasma, making the target implosion inherently susceptible to the Rayleigh-Taylor hydrodynamic instability (RTI) [1–10]. The implosion is initiated by the ablation of material from the outer shell surface with intense laser beams (direct drive) [1] or with x rays produced in a high-Z enclosure or hohlraum (indirect drive) [2]. The ablated shell mass forms a coronal plasma that surrounds the target and accelerates the shell inward via the rocket effect. Perturbations at the ablation surface that result from target imperfections, and in the case of direct drive, laser irradiation nonuniformities (i.e., laser imprint) are amplified by the ablative RTI as the shell accelerates inward [1,2]. These perturbations feed through the shell during the acceleration phase and seed the RTI of the deceleration phase at the inner shell surface [11]. When the higher-density shell converges toward the target center and is decelerated by the lower-density fuel (hot spot), the classical RTI in its highly nonlinear, turbulent stage causes atomic-scale mixing of the CH shell material or pusher with the fuel in the outer regions of the compressed core (i.e., mix region) [3]. Modulations also grow due to Bell-Plesset convergent effects throughout the implosion up to stagnation [12]. The thermonuclear fusion rate in the resulting central hot spot, which is confined by the inertia of the cold, dense shell, reaches its maximum value just before stagnation, when the fuel temperature peaks. Ultimately, the RTI can disrupt central hot spot formation in ICF and reduce the yield by mixing cold, high-density shell plasma with hot, low-density, hot spot plasma; therefore, understanding the RTI induced mix and developing ways to control it are of great importance to ICF and the ultimate goal of thermonuclear ignition in the laboratory.

The strategy to control the unstable RTI growth in direct drive ICF is to reduce the seeds and the growth rates of the dominant modes, which have been characterized in planar [4–6], cylindrical [7,8], and spherical [9,10] experiments. However, quantitative measurements of the amount of mixing caused by the RTI in ICF are not available even for the simple planar or cylindrical geometries. Measurements of the amount of shell mix in spherical implosions are essential to understand the degraded target performance that results from the RTI. The complexity of the spherical implosion makes these measurements challenging. Recently, a novel diagnostic technique that measures the density of shell material in the mix region of a spherical implosion was reported [3]. This technique is used herein to trace the shell mix back to the initial implosion conditions and to show that it correlates with the feedthrough (FT) perturbation amplitudes. This Letter shows for the first time quantitative measurements of the density of shell material in the mix region as a function of the level of FT from the ablation surface to the inner shell surface. The FT level was changed to vary the seed of the deceleration phase RTI in implosions of D_2 or DT gas filled CH shells that were designed to have similar deceleration phase RTI growth factors. A fourfold decrease in the density of shell material in the mix region of the compressed core was observed when laser imprint

levels were reduced, and the initial shell was thicker, corresponding to a reduction in the FT rms level by a factor of 6. All of the implosions in this study are predicted to have a convergence ratio of ~15 at peak compression; however, the average fuel mass densities in the core were observed to decrease as the FT levels were increased. This is evidence that the shell mix alters the trajectory of the implosion and limits the spherical compression.

RTI induced mix in spherical implosions of CH shells filled with D_2 or DT gas has been investigated [3,13–16]. Early experiments of low convergence ratio (~8), indirect drive implosions showed degraded target performance with increasing initial outer surface roughness of the capsule [16]. More quantitative RTI induced mix experiments were performed with higher convergence ratio (~15) direct drive implosions [3,13–15]. The density of shell material mixed into the outer core of direct drive CH shell spherical target implosions was estimated from time-resolved x-ray spectroscopic measurements, nuclear measurements of fuel areal density (ρR), and core x-ray images [3]. The D_2 fuel within a CH capsule was doped with trace amounts of Ar, and the emissivity-averaged core electron density (n_e) and temperature (T_e) were determined by measuring the time-dependent spectral line shapes of the Ar K-shell emissions, which probed the mix region [17]. The measured core n_e has contributions from the fuel, the Ar dopant, and the CH shell material that has mixed into the core [i.e., $n_e = n_e$ (D) + n_e (Ar) + n_e (CH)]. Time-integrated nuclear measurements of fuel ρR, which are weighted to the time of peak neutron production, were combined with x-ray core images to estimate the fuel density. Only ~50% of the measured n_e that was averaged over the neutron-burn width could be accounted for by the fuel. The contribution from the Ar dopant was negligible. It was therefore concluded that the remaining electrons must come from the CH shell material that had mixed into the core [3].

The physical picture of the compressed core at the time of peak neutron production that has emerged from RTI induced mix experiments is that a mix region, consisting of fuel and pusher material, exists in between the CH pusher and the central hot spot of fuel [e.g., see Fig. 1(b) in Ref. [3]]. The main objective of this Letter is to experimentally demonstrate with direct drive implosions the dependence of shell mix on the initial perturbation seed of the deceleration phase RTI. The seeds are the FT from the ablation surface to the inner shell surface, as well as the inner shell surface roughness. The FT levels were varied, and the mass density of CH shell material mixed with the fuel in the outer core around the time of peak neutron production by the RTI was diagnosed using the shell mix diagnostic technique of Ref. [3]. FT levels can be decreased by increasing the shell thickness of the target and by decreasing the level of laser imprint. Since all of the implosions had similar inner surface roughness, changes in the amount of shell mix were attributed to changes in the FT levels.

Spherical CH capsules containing D_2 or DT fuel were imploded on the 60-beam UV OMEGA laser system [18]. The three types of implosions that were studied are presented in Table I. All of the CH capsules had ~0.5 mm radius and 15-atm gas fill and a 20-μm shell thickness, except for the type I implosion which had 24-μm shell thickness. The targets were driven with a 23-kJ, 1-ns square laser pulse smoothed with distributed phase plates [19], 1-THz 2D smoothing by spectral dispersion (SSD) [20], and polarization smoothing (PS) using birefringent wedges [21]; however, the SSD was turned off for the type III implosion to increase the amount of laser imprint. The beam-to-beam rms power imbalance was 5% or less. The predicted convergence ratios at stagnation for the 20- and 24-μm capsules are 15 and 13, respectively. The measured primary neutron yields were in the range of 30% to 40% of the 1D predictions for these implosions [13]. Compared with type II implosions, the primary neutron yield of type III implosions dropped by ~30% when 1 THz SSD was turned off. The measured fuel areal densities are near 1D predictions for type I and II implosions [13], and are ~50% of the 1D prediction for type III implosions.

Since laser imprint levels cannot be measured directly in spherical implosions, the RTI growth at the ablation surface and the subsequent FT to the fuel-pusher interface during the acceleration phase of the shell were modeled with a postprocessor [22] to the 1D hydrodynamics code LILAC [23]. The postprocessor is based on a sharp-boundary model that takes into account time variation in the unperturbed state, mode interaction of neighboring interfaces in the target, effects of spherical convergence, and mass ablation. To account for the nonlinear saturation, Haan's 3D model [24] is applied after the mode amplitude reaches the saturation level. The perturbation spectrum due to laser imprint [25] and target imperfections (i.e., the seed for the acceleration phase) for the three types of implosions are shown in Fig. 1(a). Type III with SSD off has higher levels of laser imprint for $\ell > 15$ (the lowest ℓ mode that 1 THz SSD can smooth on OMEGA [20]) than the other two with full beam smoothing. The calculated ablation surface perturbation spectrum at the end of the acceleration phase growth is shown in Fig. 1(b). The type III implosion has a higher level of

TABLE I. Specifications for the three types of implosions.

Implosion Type	Shell Thickness (μm)	Gas Fill Pressure (atm)	Laser Beam Smoothing	Calculated Feedthrough rms (μm)
I	24	15	1 THz SSD + PS	0.3
II	20	15	1 THz SSD + PS	0.5
III	20	15	PS only	1.8

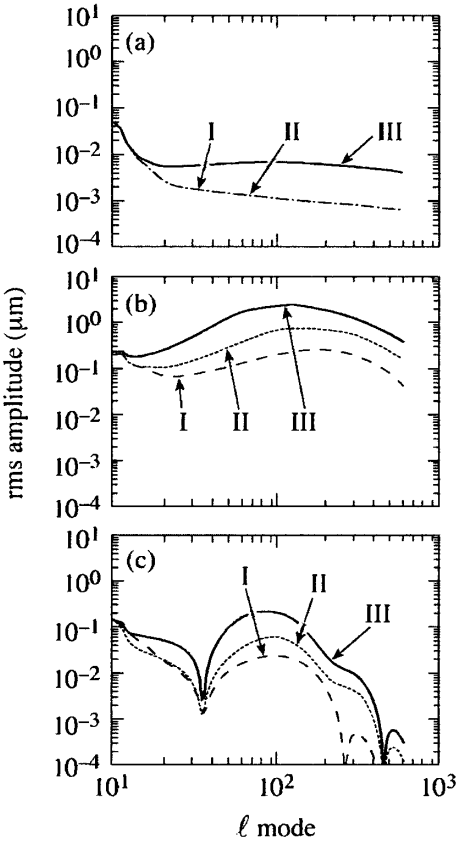

FIG. 1. Calculated levels of (a) laser imprint, (b) ablation surface perturbation at the end of the acceleration phase, and (c) feedthrough of ablation surface perturbation to fuel-pusher interface for type I (dashed line), type II (dotted line), and type III (solid line) implosions.

perturbation than type II because it started with a higher level of laser imprint. Although type I and II implosions have the same level of laser imprint, type I has less RTI growth than type II because the thicker shell travels less during the acceleration phase. For each implosion, the predicted amount of FT at the end of the acceleration phase is plotted in Fig. 1(c). The model shows that the amount of FT, and consequently the seed for the deceleration phase RTI, is highest for type III implosion and lowest for type I. As the shell thickens during the implosion the perturbations at the inner shell surface decouple from the outer shell surface and begin to oscillate. These mass oscillations give rise to the phase reversals observed in the calculated FT spectra. The calculated FT rms levels for ℓ modes greater than 10 are 0.3, 0.5, and 1.8 μm for types I, II, and III implosions, respectively. The spectrum below $\ell = 10$ was nominally the same for the implosions of this study.

The growth factor (GF) of the classical deceleration phase RTI can be expressed as $\mathrm{GF}_\ell = \exp[\gamma_\ell t]$, where $\gamma_\ell t = \sqrt{A_T \ell D/R}$. A_T, ℓ, R, and D are, respectively, the Atwood number at the fuel-pusher interface, the mode number of the perturbation, the trajectory of the fuel-pusher interface, and the distance decelerated by the fuel-pusher interface. The trajectories of the fuel-pusher interfaces were calculated with LILAC for the 20- and 24-μm shell targets. Implosions of these shells with full beam smoothing were found to have core radii near the 1D predictions [17]. A comparison of the trajectories with the free-fall lines of the fuel-pusher interface is presented in Fig. 2(a). The difference between the free-fall line and the trajectory is the distance decelerated by the fuel-pusher interface, which is plotted as a function of the trajectory in Fig. 2(b) for the 20- and 24-μm shell targets. The vertical line in Fig. 2(b) represents the radius of the fuel-pusher interface at the time of peak neutron production for the 20- and 24-μm shell targets. The time-resolved n_e measurements were averaged over the neutron-burn width, and the peak neutron production occurred later for the thicker shell target. Figure 2 shows that the implosions of the 20- and 24-μm shell targets are predicted to have the same deceleration phase RTI growth factor. Because the deceleration phase RTI is classical, the high ℓ modes quickly enter the highly nonlinear, turbulent regime. The type I implosion is expected to have the least amount of mixing because it has the least amount of FT. Conversely, the type III implosion is expected to have the most amount of mixing because it has the greatest amount of FT.

The density of shell material in the mix region averaged over the neutron-burn pulse was diagnosed using the

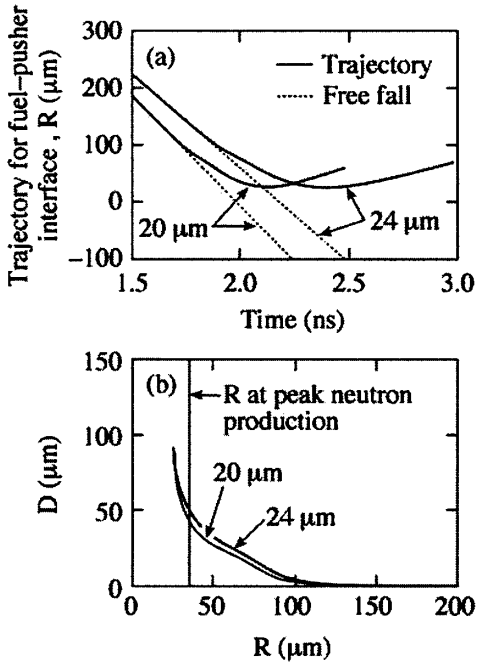

FIG. 2. Calculated (a) trajectory R and free-fall line of fuel-pusher interface for 20- and 24-μm shell implosions, and (b) distance decelerated D by fuel-pusher interface versus R. The vertical line represents R at the time of peak neutron production for 20- and 24-μm shell implosions.

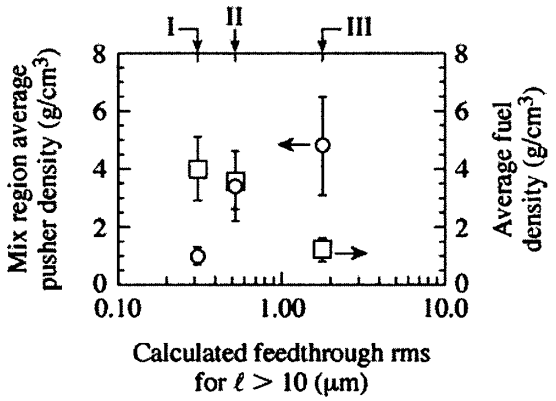

FIG. 3. Average pusher mass density (circles) in the mix region and average fuel mass density (squares) in the core around the time of peak neutron production versus the calculated FT rms levels for ℓ modes greater than 10. Implosion types I–III are labeled.

shell mix diagnostic technique of Ref. [3] for the three types of implosions. In Fig. 3 the pusher mass density (circles) in the mix region is plotted as a function of the calculated FT rms levels. These results are a compilation of data from 16 implosions. It is clearly evident that the pusher mass density in the mix region increases as the FT levels are increased. The opposite trend is observed for the average fuel mass densities (squares in Fig. 3) in the core, which decrease as the FT levels are increased. The implosion with the largest seed for the deceleration phase RTI (type III) has the highest pusher mass density in the mix region and the lowest average compressed fuel density in the core. The measured core pressures (electron + ion) averaged over the neutron-burn width for the 20-μm CH shell implosions (types II and III) are comparable at 11 ± 2.8 and 9 ± 2.3 Gbar, respectively; however, the 20-μm CH shell implosion with the lower amount of laser imprint (type II) generates this pressure at a smaller radius than the 20-μm CH shell implosions with the higher amount of laser imprint (type III). This is evidence that the shell mix limits the spherical compression of the implosion, since all of the implosions in this study are predicted to produce similar compressed fuel densities. The trajectory of the implosion is altered by the increase in core pressure caused by the shell mix and by any reduction in tamping of the deceleration phase caused by shell breakup; therefore, the fall line behavior is different for the implosion with the largest seed (type III), and the resulting RTI growth factor could be higher. Nevertheless, these results show a correlation between shell mix and the calculated FT from the ablation surface to the inner shell surface. The pusher mass density in the mix region increases by a factor of 4 and fuel mass density drops by a similar amount when the FT rms level is increased by a factor of 6. These results demonstrate how the shell mix can be controlled by varying the initial implosion conditions of laser imprint and shell thickness and how the shell mix can limit the spherical compression of the implosion.

In conclusion, this Letter experimentally showed the mixing of cold, high-density shell plasma with the low-density, hot spot plasma by the RTI in ICF correlated with the calculated FT from the ablation surface to the inner shell surface. A fourfold decrease in the density of shell material in the mix region of direct drive implosions of gas filled spherical CH shells having convergence ratios $\sim$15 was observed when the FT rms level was reduced by a factor of 6. These results demonstrate how the shell mix can be controlled by varying the initial implosion conditions of laser imprint and shell thickness and how the shell mix can limit the spherical compression of the implosion.

This work was supported by the U.S. Department of Energy Office of Inertial Confinement Fusion under Cooperative Agreement No. DE-FC03-92SF19460, by the University of Rochester, and by the New York State Energy Research and Development Authority.

*Also at Departments of Mechanical Engineering, and Physics and Astronomy.

[1] S. E. Bodner *et al.*, Phys. Plasmas **5**, 1901 (1998).
[2] J. D. Lindl, *Inertial Confinement Fusion* (Springer, New York, 1998).
[3] S. P. Regan *et al.*, Phys. Rev. Lett. **89**, 085003 (2002).
[4] V. A. Smalyuk *et al.*, Phys. Rev. Lett. **81**, 5342 (1998).
[5] C. J. Pawley *et al.*, Phys. Plasmas **6**, 565 (1999).
[6] S. G. Glendinning *et al.*, Phys. Rev. Lett. **78**, 3318 (1997).
[7] G. Dimonte, Phys. Plasmas **6**, 2009 (1999).
[8] W.W. Hsing *et al.*, Phys. Plasmas **4**, 1832 (1997).
[9] S. G. Glendinning *et al.*, Phys. Plasmas **7**, 2033 (2000).
[10] V. A. Smalyuk *et al.*, Phys. Rev. Lett. **87**, 155002 (2001).
[11] M. M. Marinak *et al.*, Phys. Plasmas **3**, 2070 (1996).
[12] G. I. Bell, Los Alamos Scientific Laboratory Report No. LA-1321, Los Alamos, 1951); M. S. Plesset, J. Appl. Phys. **25**, 96 (1954).
[13] D. D. Meyerhofer *et al.*, Phys. Plasmas **8**, 2251 (2001).
[14] P. B. Radha *et al.*, Phys. Plasmas **9**, 2208 (2002).
[15] C. K. Li *et al.*, Phys. Rev. Lett. **89**, 165002 (2002).
[16] T. R. Dittrich *et al.*, Phys. Rev. Lett. **73**, 2324 (1994).
[17] S. P. Regan *et al.*, Phys. Plasmas **9**, 1357 (2002).
[18] T. R. Boehly *et al.*, Opt. Commun. **133**, 495 (1997).
[19] Y. Lin, T. J. Kessler, and G. N. Lawrence, Opt. Lett. **21**, 1703 (1996).
[20] S. Skupsky and R. S. Craxton, Phys. Plasmas **6**, 2157 (1999).
[21] T. R. Boehly *et al.*, J. Appl. Phys. **85**, 3444 (1999).
[22] V. N. Goncharov *et al.*, Phys. Plasmas **7**, 5118 (2000).
[23] M. C. Richardson *et al.*, in *Laser Interaction and Related Plasma Phenomena*, edited by H. Hora and G. H. Miley (Plenum, New York, 1986), Vol. 7, p. 421.
[24] S.W. Haan, Phys. Rev. A **39**, 5812 (1989).
[25] T. R. Boehly *et al.*, Phys. Plasmas **8**, 2331 (2001).